

Microwave synthesis of In-doped TiO₂ nanoparticles for photocatalytic application

M. B. Suwarnkar¹ · G. V. Khade¹ · S. B. Babar¹ · K. M. Garadkar¹

Received: 3 June 2017 / Accepted: 2 August 2017 / Published online: 5 August 2017
© Springer Science+Business Media, LLC 2017

Abstract The present work reports on pristine anatase TiO₂ photocatalyst with different indium (In) content which is prepared via a controlled and energy efficient microwave-assisted method. The structural and optical properties of photocatalyst were characterized by X-ray diffraction (XRD), field emission-scanning electron microscopy (FE-SEM), energy dispersive spectroscopy (EDS), transmission electron microscopy (TEM), diffuse reflectance spectroscopy (DRS), and fourier transform infrared spectroscopy (FT-IR). Average crystallite size of 12 nm with shape of pseudo-cube was obtained for In-doped TiO₂ (optimum 0.10 mol%). The UV–Vis diffuse reflectance spectrum shows the absorption edge which is shifted in the visible region and slightly decreased the band gap for In–TiO₂ as compared to pristine TiO₂. The present research work is mainly focused on the enhancement of degradation efficiency of methyl orange (MO) by doping of Indium in TiO₂ using UV light (365 nm). A 98% efficiency of photodegradation was achieved by utilizing 0.10 mol% In-doped TiO₂ (1 g/dm³) at pH=5 within 90 min. Recyclability of photocatalyst was also studied and material found to be stable up to five runs.

1 Introduction

Nowadays the environmental protection is one of the most promising objectives of the humanity. Water pollution is mostly occurred due to industrial effluents discharged

directly into the water bodies. Wastewater recycling is one of the effective solution for water shortage in many water-salvage countries; however, waterborne pathogens limit the reusing by infecting the contacting people and threatening human health, especially for developing countries [1]. Dyes are widely used in the textile, rubber, paper, plastic, and cosmetic industries. Due to discharge of synthetic dye-containing wastewater, the effective treatment of dyes and organic substances containing wastewater has been intensely studied [2].

Many techniques are employed for wastewater treatment such as physical separation method, biodegradation method, and photocatalysis. Among these, photocatalysis is a promising method used in degradation of different dyes and organic pollutants. The principle of photocatalysis involves the mineralization of organic compounds into CO₂ and H₂O by using the UV and Vis irradiation in presence of semiconductor.

Semiconductors like ZnO, TiO₂ have great importance in the field of Nanoscience and Nanotechnology due to their broad and interdisciplinary area of research. The photocatalytic activity of nonmaterial is enhancing than that of bulk material and that has been studied worldwide in the last few decades [3]. In the field of nanomaterials, many of the Scientists are attracted due to its wide range of applications in different fields like hydrogen generation [4], gas sensors [5], dye-sensitized solar cells [6], photovoltaic cells [7], semiconductors [8–12], photocatalysis [13, 14], self-cleaning [15] and antimicrobial and antifungal activity [16].

Among various metal oxides, Titania is one of the most widely used benchmark standard photocatalyst in the field of environmental cleaning application. It is a non-toxic material, with stable in nature and low cost [17]. However, the large band gap of TiO₂ and massive recombination of

✉ K. M. Garadkar
kmg_chem@unishivaji.ac.in

¹ Nanomaterials Research Laboratory, Department of Chemistry, Shivaji University, Kolhapur 416004, India

photogenerated charge carrier species limit its overall photocatalytic efficiency. Regarding its properties, TiO_2 is a semiconductor with a band gap of about 3.2 eV allowing light absorption in UV region (about 5% of solar spectrum). However, the absorption of only a small fraction of the solar spectrum makes TiO_2 not enough for practical applications. Additionally, the electron–hole recombination is considered a serious problem for its photocatalytic performance, since this process limits drastically the TiO_2 quantum yield [18]. The former can be overcome by modifying the electronic band structure of titania including various strategies like coupling with a narrow band gap semiconductor, metal ion/non-metal ion doping, co-doping with two or more foreign ions, surface sensitization by organic dyes or metal complexes, and noble metal deposition [19].

Shchukin et al. [20] prepared nanocrystalline $\text{TiO}_2\text{--In}_2\text{O}_3$ powders with various Ti/In ratios by sol–gel technique using indium(III) nitrate and TiCl_4 are the precursors and evaluated their photocatalytic activity for degradation of aqueous 2-chlorophenol. Poznyak et al. [21] prepared $\text{TiO}_2\text{--In}_2\text{O}_3$ composites by the sol–gel technique from concentrated hydrous titanium dioxide and indium hydroxide sols and studied their structural, optical and photoelectrochemical properties. Gonzalez and co-workers [22] reported the synthesis, characterization and photocatalytic properties of $\text{TiO}_2\text{--In}_2\text{O}_3$ catalyst. Compared with pure TiO_2 , $\text{TiO}_2\text{--In}_2\text{O}_3$ composite photocatalyst showed an efficient separation of photogenerated carriers and observed an enhancement in photocatalytic activity under UV irradiation [20–22]. Wang et al. [23] prepared indium doped TiO_2 by the sol–gel method by using titanium(IV) tetrabutoxide and indium chloride are the precursors. The pure TiO_2 photocatalyst shows only 8.2% of degradation of 4-chlorophenol after 8 h, whereas optimized In– TiO_2 shows 38.8% after 8 h under the visible light. The indium doped TiO_2 showed improved photocatalytic activity for degradation of 4-chlorophenol compared to pure TiO_2 .

In the present study, we illustrate the doping of TiO_2 with indium by an energy efficient microwave assisted method. The synthesized nanomaterials were thoroughly characterized by several techniques to predict the structure and composition. The photocatalytic activity of the catalyst was evaluated by using methyl orange as a model pollutant. In order to achieve maximum photocatalytic activity, a series of experiments were carried out which includes the doping content of Indium, the effect of catalyst loading, and pH.

2 Experimental

2.1 Materials

Titanium tetra-isopropoxide (TTIP, 99%), surfactant cetyl trimethyl ammonium bromide (CTAB, 99%) were

purchased from Spectrochem Pvt. Ltd., (India). Sodium dodecyl sulfate (SDS, extrapure) was purchased from Thomas Baker Pvt. Ltd., Mumbai. Absolute ethanol (99.9%) and indium nitrate were purchased from s.d. fine chemicals. Ammonia was purchased from Loba Chemie Pvt. Ltd., (India). All analytical grade chemicals were used as received for preparation of various solutions. All solutions were prepared in Millipore water obtained from Millipore water system (Bangalore, India).

2.2 Preparation of indium doped TiO_2 nanoparticles

Titanium tetra-isopropoxide and indium nitrate were used as a source of titanium and indium respectively. In doped TiO_2 nanocrystalline powder was prepared by controlled addition of (0.1 M) TTIP in 100 mL of absolute ethanol with constant stirring to get a clear solution. Further, a sufficient amount of surfactant solution (1% CTAB + 1% SDS) was added with constant stirring. For indium doping, the concentration of In was varied from 0.05 to 0.2 mol%. The required amount of (0.1 M) indium nitrate was added to get the desired composition. An aqueous ammonia was added drop wise under stirring condition with special arrangement at room temperature until the solution reached up to pH=8. After complete precipitation, the precipitate was washed with Millipore water and acetone for several times to remove excess surfactant. The washed precipitate was kept under microwave irradiation for 20 min in the domestic microwave oven (Input 900 W, 250 MHz, LG Make) with on–off cycle (20 s on–40 s off). The dried powder was grounded by using agate mortar and pestle and calcined at 300 °C for 3 h in a temperature controlled muffle furnace. Nanocrystalline powder of pristine TiO_2 was prepared similarly without addition of In source. The phase purity and degree of crystallinity of the TiO_2 and effect of In doping were monitored by XRD.

2.3 Characterization of indium doped TiO_2

Powder X-ray diffraction patterns of pristine and doped TiO_2 were obtained using an XRD (Model X-Pert PRO-1712) with $\text{CuK}\alpha$ radiation ($\lambda=1.5406$ Å) as an X-ray source. The morphological investigation was carried out by a FE-SEM (TESCAN MIRA3). The EDS was recorded in the binding energy region of 0–10 keV (Model X-Act, Oxford) instrument. The shape and size of the materials was obtained by using transmission electron microscopy with model TEM (JEOL 3010). The diffuse reflectance spectra were recorded on UV–Vis Spectrophotometer (3092). FT-IR spectra were scanned using KBr pellet, with a Perkin–Elmer spectrometer (Spectrum BX-II).

2.4 Photocatalytic activity of indium doped TiO₂

The photocatalytic activity of In-doped TiO₂ was evaluated by testing the degradation of MO as a model pollutant by using UV light (365 nm). To search the highest photocatalytic activity of In-doped TiO₂, catalyst amount was varied from 0.5 to 2 g/dm³. The effect of pH on the photocatalytic activity was also studied by varying the pH of the solution from 5 to 9 by using HCl and NaOH (1 M each). The quartz photoreactor was kept in steel container along with magnetic stirrer. Philips (HPL-N, 250 W) light source was used which has Lumens of 12,750. The outer side of the bulb was broken and just inside filament is used as a source of light. The distance of lamp was kept 5 cm above the dye solution. In the given experiment the photocatalyst was added in photoreactor containing methyl orange (100 mL, 20 ppm). Prior to irradiation, dye solution was stirred for 30 min in dark for adsorption–desorption equilibrium.

3 Result and discussion

3.1 Characterization of as prepared In–TiO₂

3.1.1 XRD

The mechanism of modification is closely related to the crystallite structure, which has been studied using the XRD technique. To examine the changes in the crystal structure of TiO₂ affected by In doping, XRD analysis was carried out in the range of $2\theta = 10^\circ$ – 90° . Figure 1 shows X-ray diffraction pattern of pristine and different contents of In from 0.05 to 0.20 mol%. All the samples exhibit the anatase structure even after the doping of indium. The strong diffraction peaks at 25.06° , 37.59° , 48.01° , 54.05° , 55.02° , 62.31° , 69.94° and 74.92° associated to the crystal planes [101], [004], [200], [105], [211], [204], [220] and [215] respectively, this attributed to reflections of anatase TiO₂ which is compared with JCPD Card No. (21–1272) [24]. The space group of anatase TiO₂ is $I4_1/amd$ with lattice constant $a = 3.7845 \text{ \AA}$, $c = 9.5153 \text{ \AA}$ (where $a = b \neq c$). As the Indium content increases from 0.05 to 0.10 mol%, the peak broadening [101] gradually increases which indicates that the crystallite size of the material is smaller. The contents of In is too low and could not be detected by XRD. The average crystallite size of the material was calculated by using Scherrer's equation [25]. It is observed that the pristine TiO₂ has an average size of 15 nm and it decreases up to 12 nm for 0.10 mol% In doping. Hence as doping amount increases the peaks of TiO₂ became slightly broad in width which leads to the reduction of crystallite size. The reduction in size by doping suggests that doping of Indium inhibits the growth of TiO₂ crystallite.

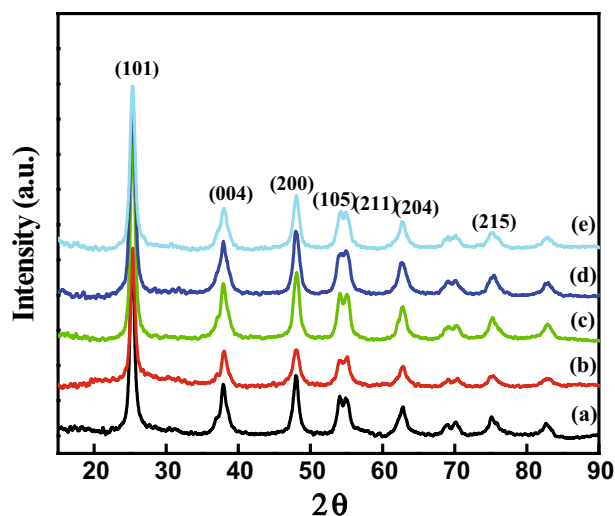


Fig. 1 X-ray diffractograms of *a* TiO₂, *b* In–TiO₂ (0.05 mol%), *c* In–TiO₂ (0.10 mol%), *d* In–TiO₂ (0.15 mol%) and *e* In–TiO₂ (0.20 mol%) nanoparticles

It is reported that there are two kinds of doping modes such as interstitial and substitutional, for doping of metal ions in metal oxides [26]. In case of first interstitial mode, the ionic radius of dopant should be smaller than that of the lattice metal ion and the oxide lattice spacing, allowing the doping metal ions to penetrate into the crystal cell of the metal oxide. The ionic radius of the In³⁺ ion (81 pm) [27] is larger than that of the lattice Ti⁴⁺ ion (53 pm) [26], it is impractical for the In³⁺ ions to penetrate into the crystal cell of pristine TiO₂ through the interstitial mode. On doping with the substitutional mode, the doping of metal ions will substitute the lattice metal ions and thus occupy the position of the lattice metal ions in the metal oxide. If the ionic radius of the doping metal ion is larger than that of the lattice ion, the lattice parameters and cell volume of the doped oxide should be larger than those of the pure metal oxide. As a result, the positions of all of the diffraction peaks in XRD patterns should shift to lower diffraction angles. It is observed that no shifting of the peaks from XRD diffraction pattern of In–TiO₂, as shown in Fig. 1. Therefore, the doping of In³⁺ ions into TiO₂ through the substitutional mode can also be excluded. Thus, it is reasonable to suppose that the In³⁺ metal ions are doped on the surface of pristine TiO₂. Furthermore, the microstrains of the In-doped TiO₂ samples were determined by the following formula to confirm the doping mode [28].

$$\text{Microstrain } (\varepsilon) = \frac{\beta}{4 \tan \theta} \quad (1)$$

where β is FWHM in radian,

After calculation of microstrain, it is observed that pristine TiO₂ shows 5.7×10^{-3} and In–TiO₂ (0.10 mol%)

6.2×10^{-3} respectively. The result indicates that there is a very small change in microstrain which agrees that the In atoms are on the surface of TiO_2 .

3.1.2 EDS and FE-SEM analysis of In– TiO_2

In order to investigate the surface morphology of the synthesized In doped TiO_2 nanoparticles, FE-SEM studies were performed. Figure 2a shows FE-SEM image of 0.10 mol% In– TiO_2 which indicates that the particles of nearly uniform in size with spherical morphology. To check the elemental composition present in In– TiO_2 , EDS were recorded and pattern is shown in Fig. 2b. The spectrum was recorded in the binding energy region of 0–10 keV. The spectrum demonstrates the number of well defined peaks at 0.4, 4.5, 4.9, 0.5 and 3.5, 4.2 keV relative to Ti, O and In respectively, which clearly supports the presence of Ti, O and Indium in the material. In the spectrum no other peaks were detected which confirm the purity of nanomaterial. The atomic% of Ti, O and In are 32.16, 67.45 and 0.39 respectively, which indicates that the material formed were of non-stoichiometric with oxygen deficiency that leads to better performance of photocatalytic activity [29].

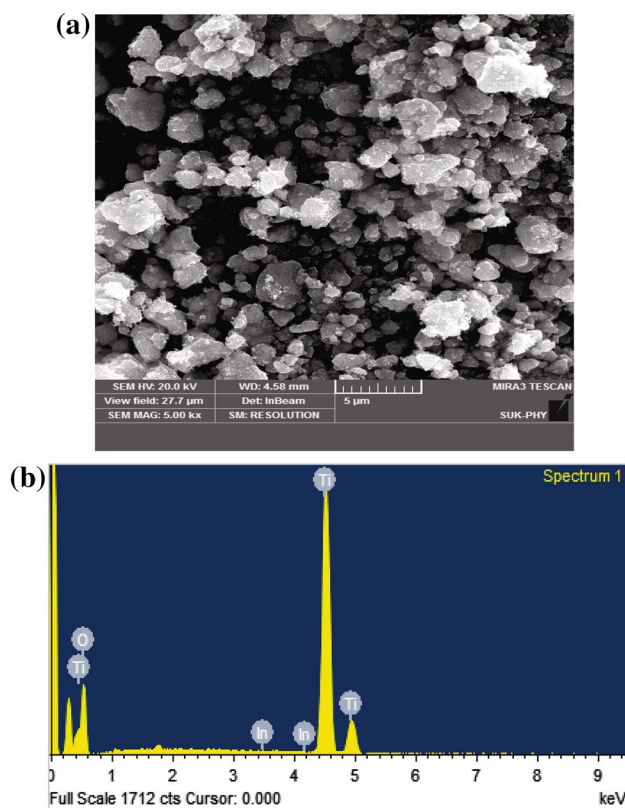


Fig. 2 a FE-SEM of 0.1 mol% In– TiO_2 . b EDS of 0.1 mol% In– TiO_2

3.1.3 TEM

Morphology of the nanomaterials was characterized by TEM analysis (Fig. 3). The obtained image reveals that as prepared In– TiO_2 is in the form of pseudo spherical in shape with narrow size distribution. The size of particles is in the range of 10–15 nm, with the average particle size from representative TEM was found to be 12 nm. The HR-TEM image (Fig. 3c) shows lattice fringes, which is used for phase identification and found to be 0.35 nm, this value corresponds to the lattice spacing of (101) plane in the anatase phase. Selected area electron diffraction pattern (SAED) matches to anatase phase with good crystallinity as shown in Fig. 3d. Lattice fringes from SAED can be clearly indicating that the particles are crystalline in nature with anatase phase.

3.1.4 Diffuse reflectance spectra

Figure 4 shows the diffuse reflectance spectra of pristine TiO_2 and In– TiO_2 with varying Indium contents from 0.05 to 0.20 mol%, after being calcined at 300 °C for 3 h. It was observed that the absorption onset of In– TiO_2 slightly shifted towards the visible region [23]. This is due to formation of metal cluster that gives rise to localized energy in the band gap. Particularly the 0.10 mol% In-doped TiO_2 shifted towards red region indicating the decrease in band gap as compared to pristine TiO_2 .

3.1.5 FT-IR spectra

The FT-IR spectra of pristine TiO_2 and In– TiO_2 nanoparticles with varying mol% of In from 0.05 to 0.20 mol% after being calcined at 300 °C for 3 h are shown in Fig. 5. The spectrum (a) shows a broad band centered at 3420 cm^{-1} , which is ascribed to –OH stretching and band at 1634 cm^{-1} due to the –OH bending mode of water adsorbed on the surface of the TiO_2 which may have the essential role in the photocatalytic activity. The methylene symmetric and antisymmetric vibrations can be seen in the area of $2930\text{--}2830 \text{ cm}^{-1}$ which arises due to the surfactants. The broad peak at $725\text{--}685 \text{ cm}^{-1}$ is the feature of the Ti–O bending mode of vibrations which indicates the creation of metal–oxygen bonding [30]. The In–O stretching at the wavenumber 557 cm^{-1} was not observed hence it can be concluded that there was no formation of In_2O_3 [31]. The intensity of bands at 1634 and 725 cm^{-1} shift towards lower wavenumber after In doping, indicating the formation of In– TiO_2 composite.

Fig. 3 TEM image **a** In doped TiO₂ (50 nm), **b** In doped TiO₂ (20 nm), **c** HRTEM image of In doped TiO₂, **d** SAED pattern of In doped TiO₂

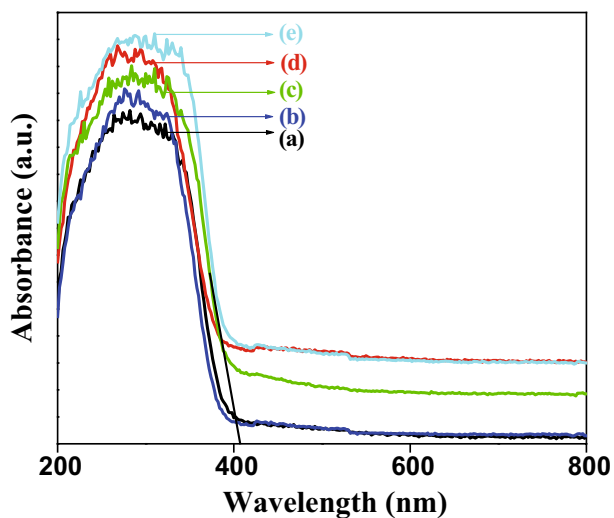
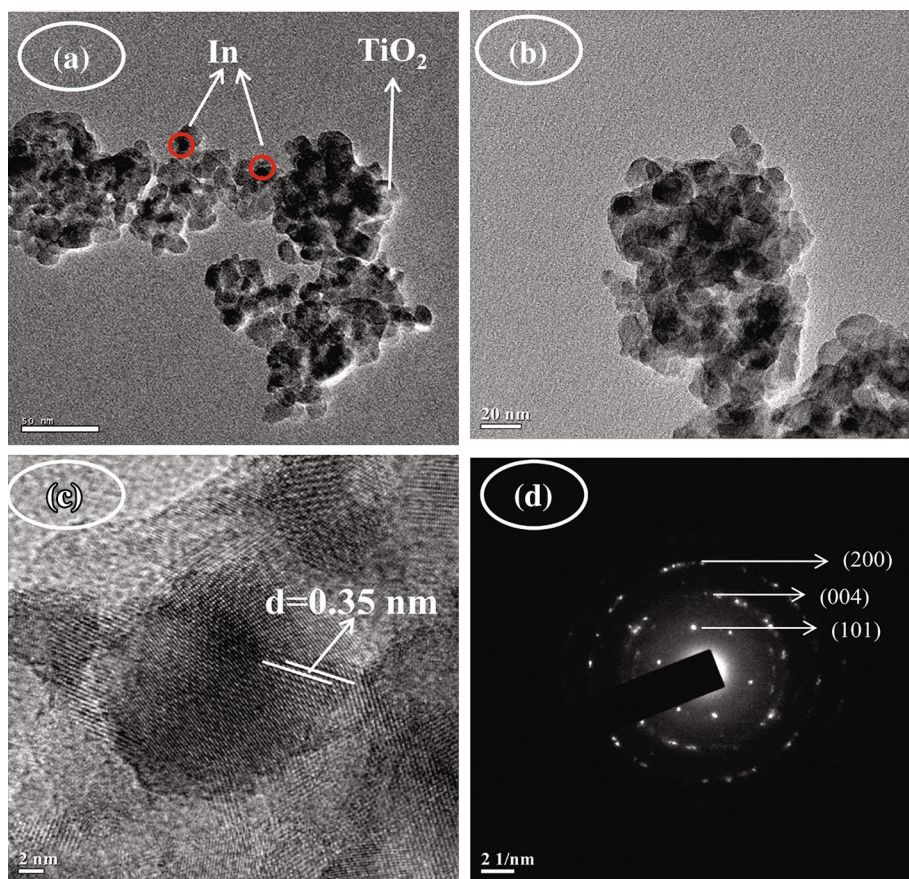


Fig. 4 Diffuse reflectance spectra of *a* TiO₂, *b* In-TiO₂ (0.05 mol%), *c* In-TiO₂ (0.10 mol%), *d* In-TiO₂ (0.15 mol%) and *e* In-TiO₂ (0.20 mol%) nanoparticles

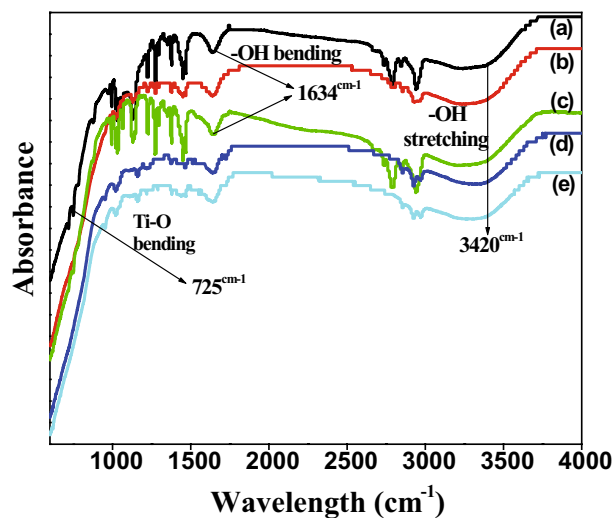


Fig. 5 FT-IR spectra of *a* TiO₂, *b* In-TiO₂ (0.05 mol%), *c* In-TiO₂ (0.10 mol%), *d* In-TiO₂ (0.15 mol%) and *e* In-TiO₂ (0.20 mol%) nanoparticles

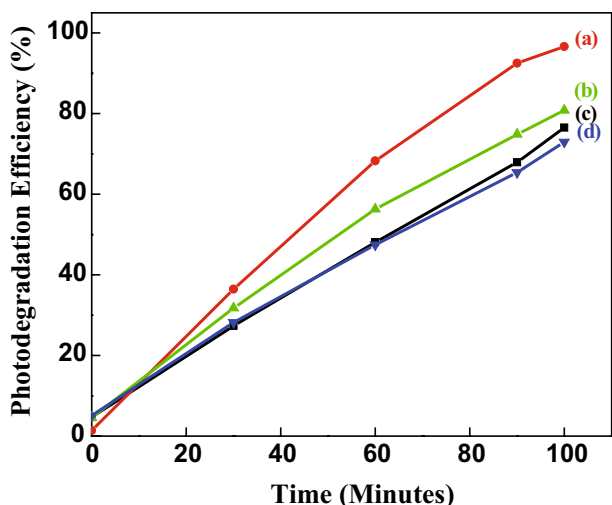


Fig. 6 Effect of In doping in TiO₂ nanoparticles a In-TiO₂ (0.10 mol%), b In-TiO₂ (0.15 mol%), c In-TiO₂ (0.20 mol%) and d In-TiO₂ (0.05 mol%) nanoparticles

3.2 Factors affecting on photocatalytic degradation of methyl orange

3.2.1 Effect of concentration on Indium doping

The photodegradation of MO was employed to evaluate the photocatalytic activity of In-TiO₂ under UV light. The experimental results are illustrated in Fig. 6. Initially, the degradation efficiency of MO increases as the content of Indium increases on TiO₂. The 0.1 mol% In-TiO₂ shows maximum photocatalytic activity by keeping other experimental parameters constant. It may be due to increase in number of active sites, recombination rate of electron and holes decreases and hence 0.1 mol% In-TiO₂ shows higher photocatalytic performance. However as doping increased from 0.1 mol%, the activity was more or less constant. The reason is that the aggregation of Indium nanoparticles became serious when more In was introduced into the TiO₂.

3.2.2 Effect of catalyst loading for methyl orange degradation

The effect of catalyst loading on the degradation of methyl orange was investigated using optimal (0.10 mol%) In-doped TiO₂ nanoparticles. In photocatalysis process the amount of photocatalyst is an important factor quantitatively. Hence a series of experiments were carried out to find the optimal content of indium doped TiO₂ for degradation of MO. The quantity of photocatalyst was varied from 0.5 to 2 g/dm³ keeping all other experimental parameters identical and shown in Fig. 7. It was observed that

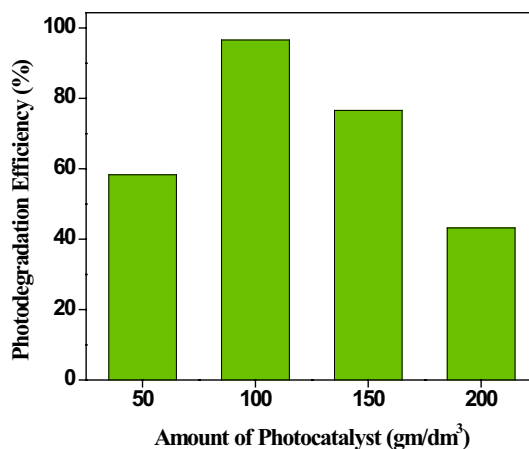


Fig. 7 Effect of catalyst loading on MO photodegradation

initially, the degradation efficiency increases with increase in the amount of photocatalyst. With 1 g/dm³ catalyst, the dye degradation efficiency was found to be high and then decreases even though catalyst amount of photocatalyst increases. This study can be explained in terms of the number of active sites existing for photocatalytic reactions. It was observed that a large amount of catalyst may affect in agglomeration of catalyst. This reduces the number of active sites [32]. Another reason for decreased degradation efficiency can be attributed to the enhancement in the turbidity of suspension causes scattering of light which leads to the inhibition of photon absorption.

3.2.3 Effect of initial pH

The pH of solution is an important parameter in the photocatalytic processes, since it not only plays an important

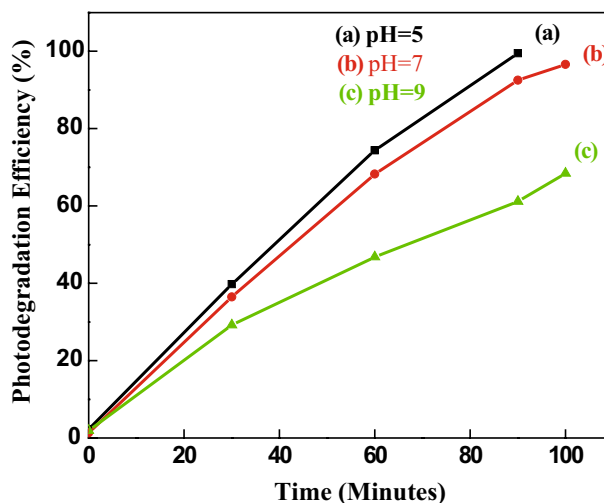
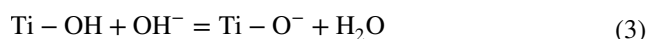
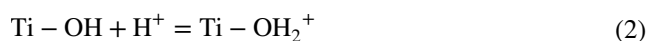


Fig. 8 Effect of pH on photodegradation of MO

role on the characteristics of wastewater treatment but also determines the surface charge properties of a photocatalyst, the charge of dye molecules, the dye adsorption ability on a photocatalyst surface, and the concentration of hydroxyl radicals available in a system [33]. In order to investigate the effect of pH on degradation efficiency, the experiments were carried out at different pH ranging from 5 to 9 for dye concentration (20 ppm) and catalyst loading (1 g/dm³). Figure 8 shows the photocatalytic activity of In–TiO₂ nanoparticles with different pH. The highest 98% photodegradation efficiency was obtained at pH=5 within 90 min. under UV-light irradiation. The amphoteric behavior of synthesized oxide influences the surface charge of the photocatalyst. The pH of dye solution can vary with the surface charge of the photocatalyst and also shifts the position of redox reaction [34, 35]. Due to amphoteric nature of TiO₂, the following two equilibriums are considered:



From reactions (2) and (3) the surface of photocatalyst has become positively charged in acidic medium while negatively charged in alkaline medium. Methyl orange is an anionic dye; after ionization, it pays attention towards the surface of the photocatalyst. At pH 5, it shows maximum photocatalytic activity due to electrostatic attraction between the anionic dye and positively charged TiO₂ surface. At pH >7, the surface of the catalyst has become negatively charged that leads to electrostatic repulsion between MO and catalyst which results in the decrease of degradation efficiency.

Repeatedly use of photocatalyst is one of the key concept for economically viable in wastewater management. To check the reusability of In–TiO₂ (0.10 mol%) for photocatalysis under UV light irradiation, the catalyst was

frequently used for five times as shown in Fig. 9. After each repeated experiment, the catalyst was collected by centrifugation and washed with distilled water and ethanol until a clear supernatant was obtained. The washed catalyst was dried at 70 °C for 60 min. and again used for the degradation of MO. The result indicates that the catalyst was reusable (at least for five runs) and proves the reusability of photocatalyst.

4 Conclusions

In summary, the TiO₂ nanomaterials with different In mol% have been synthesized by using a simple, eco-friendly, energy efficient and cost effective microwave-assisted method. The average particle size of nanomaterials was found to be 12 nm with highly crystalline pure anatase phase which was in good agreement with the results obtained from XRD and TEM. The UV–Vis diffuse reflectance spectrum showed the absorption edge which was shifted in the visible region and slightly decreases in the band gap of optimal In–TiO₂ as compared to pristine TiO₂. The atomic% of Ti, O and In are 32.16, 67.45 and 0.39 respectively, which indicates that the material formed were of non-stoichiometric with oxygen deficiency. It was found that a 98% MO was degraded within 90 min. when 1 g/dm³ In-doped TiO₂ was added to Methyl orange at pH=5 under UV-light. A 20% increment in degradation was obtained compared to TiO₂ and these are better results than pristine TiO₂. The catalyst was reused up to five runs and found to be stable without loss of activity.

Acknowledgements Authors are thankful to DST, New Delhi for financial support under Major Research Project (SR/S1/PC/0041/2010). Authors are also thankful to SAIF-NEHU, Shillong for providing TEM Facility.

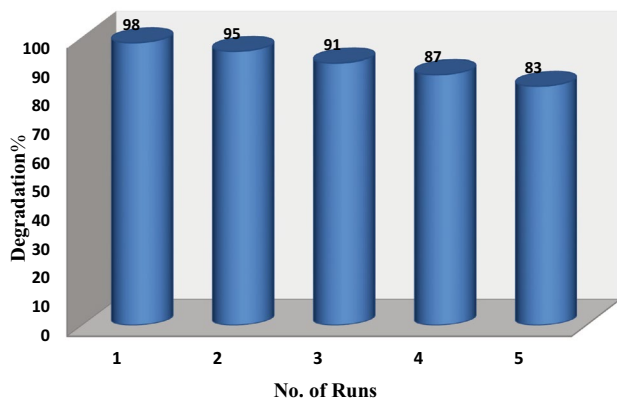


Fig. 9 Reusability of photocatalyst for degradation of MO

References

1. H. Wang, P. Jia, N. Ding, G. Pang, N. Wang, *Water Air Soil Pollut.* **226**, 333 (2015)
2. A. Peter, A.M. Cozmuta, C. Nicula, L.M. Cozmuta, A. Jastrzębska, A. Olszyna, L. Baia, *Water Air Soil Pollut.* **228**, 41 (2017)
3. R. Fagana, D.E. McCormack, D.D. Dionysiou, S.C. Pillai, *Mater Sci Semicond Process.* **42**, 2 (2016)
4. A. Kmetyko, K. Mogyrosi, V. Gerse, Z. Konya, P. Pusztai, A. Dombi, K. Hernadi, *Materials* **7**, 7022–7038 (2014)
5. Y. Zhang, S. Guo, Z. Zheng, *J. Exp. Nanosci.* **8**, 184–193 (2013)
6. H. Chen, W. Fu, H. Yang, P. Sun, Y. Zhang, L. Wang, W. Zhao, X. Zhou, H. Zhao, Q. Jing, X. Qi, Y. Li, *Electron. Act.* **56**(2), 919–924 (2010)

7. A. Nabok, *Organic and Inorganic Nanostructures*. (Artech Publishing House, London, 2005)
8. L.D. Marco, M. Manca, R. Giannuzzi, F. Malara, G. Melcarne, G. Ciccarella, I. Zama, R. Cingolani, G. Gigli, *J. Phys. Chem. C* **114**, 4228–4236 (2010)
9. T.L. Thompson, J.T. Yates, *Chem. Rev.* **106**, 4428–4453 (2006)
10. A. Kudo, Y. Miseki, *Chem. Soc. Rev.* **38**, 253–278 (2009)
11. D.R. Baker, P.V. Kamat, *Adv. Funct. Mater.* **19**, 805–811 (2009)
12. Q. Zhang, W. Fan, L. Gao, *Appl. Catal. B* **76**, 168–173 (2007)
13. P.P. Hankare, R.P. Patil, A.V. Jadhav, K.M. Garadkar, R. Sasi-kala, *Appl. Catal. B* **107**, 333–339 (2011)
14. F. Taleshi *J Mater Sci.* **26**, 3262–3267 (2015)
15. M.G. Krishna, M. Vinjanampati, D.D. Purkayastha, *Euro. Phys. J. Appl. Phys.* **62**, 30001 (2013)
16. S.M. Dizaj, F. Lotfipour, M.B. Jalali, M.H. Zarrintan, K. Adib-kia, *Mater. Sci. Eng. C* **44**, 278–284 (2014)
17. M.B. Suwarnkar, A.N. Kadam, G.V. Khade, N.L. Gavade, K.M. Garadkar, *J. Mater. Sci.* **27**, 843–851 (2016)
18. M. Popa, E. Indrea, P. Pascuța, V. Coșoveanu, I.C. Popescu, V. Danciu, *Rev. Roum. Chim.* **55**, 369–375 (2010)
19. E. Wang, P. Zhang, Y. Chen, Z. Liu, T. He, Y.J. Cao, *Mater. Chem.* **22**, 14443–14449 (2012)
20. D. Shchukin, S. Poznyak, A. Kulak, P. Pichat, *J. Photochem. Photobio. A* **162**, 423–430 (2004)
21. S.K. Poznyak, D.V. Talapin, A.I. Kulak, *J. Phy. Chem. B* **105**, 4816–4823 (2001)
22. V.R. Gonzalez, A.M. Rodriguez, M. May, F. Tzompantzi, R.J. Gomez, *Photochem. Photobio. A* **193**, 266–270 (2008)
23. E. Wang, W. Yang, Y.J. Cao, *Phy. Chem. C.* **113**, 20912–20917 (2009)
24. J.V. Smith (ed), *X-ray Powder Data File*. (American Society for Testing Materials, Pennsylvania, 1960)
25. B.M. Reddy, I. Ganesh, A. Khan, *Appl. Catal. A* **248**, 169–180 (2003)
26. Y. Cao, W. Yang, W. Zhang, G. Liu, P. Yue, *New J. Chem.* **28**, 218 (2004)
27. H. Okushita, T. Shimidzu, *Bull. Chem Soc Jpn.* **63** 920 (1990)
28. P.K. Labhane, L.B. Patle, V.R. Huse, G.H. Sonawane, S.H. Sonawane, *Chem. Phy. Lett.* **661** 13–19 (2016)
29. G. Liu, H.G. Yang, X. Wang, H. Cheng, H. Lu, L. Wang, G.Q. Lu, H.M. Cheng, *J. Phys. Chem.* **113**, 21784 (2009)
30. A.N. Murashkevich, A.S. Lavitskaredrafya, T.I. Barannikova, I.M. Zharskii, *J. Appl. Spectro.* **75**, 730–734 (2008)
31. S. Harinath Babu, N. Madhusudhana Rao, S. Kaleemulla, G. Amarendra, C. Krishnamoorthi, *Bull. Mater. Sci.* **40**, 17–23 (2017)
32. G.V. Khade, M.B. Suwarnkar, N.L. Gavade, K.M. Garadkar, *J. Mater. Sci.* **27**, 6425–6432 (2016)
33. S.S. Mandal, A.J. Bhattacharyya, *J. Chem. Sci.* **124**, 969–978 (2012)
34. V. Mirkhani, S. Tangestaninejad, M. Moghadam, M.H. Habibi, A. Rostami-Vartooni, *J. Iran. Chem. Soc.* **6**, 578–587 (2009)
35. X. Wang, P. Li, X.X. Han, Y. Kitahama, B. Zhao, Y. Ozaki, *Nanoscale* (2017). doi:[10.1039/C7NR03839A](https://doi.org/10.1039/C7NR03839A)